Wavelength Calibration Correction Technique for Improved Emissivity Retrieval

Michael Pieper, Dimitris Manolakis, *Life Fellow, IEEE*, Eric Truslow, Andrew Weisner, Randall Bostick, and Thomas Cooley

***Abstract*—Accurate retrieval of surface emissivity from long-wave infrared hyperspectral imaging data is necessary for many scientific and defense applications. Emissivity retrieval requires an atmospheric model for the scene and consists of two interwoven steps: atmospheric compensation (AC) and temperature–emissivity separation (TES). AC converts the at-aperture radiance to ground radiance, and TES uses the ground radiance to produce a temperature and emissivity estimate. TES assumes that emissivity spectra for solids are smooth, compared to atmospheric features. Model-based techniques find an atmospheric model, which produces the smoothest emissivity estimates. The high-resolution model must be band averaged to the sensor's spectral response function (SRF), which is difficult to characterize and maintain. Any errors in the SRF cause errors in the atmospheric spectra and roughness in the emissivity estimates. We propose a technique that improves the quality of the retrieved emissivity by correcting band-averaging errors of the model from the SRF. An in-scene AC (ISAC) technique is used to find pixels containing a high emissivity material. Atmospheric model bands far from absorption features and a material library are then used to identify the material and estimate the pixel temperatures. At-aperture radiance spectra are generated for the pixels, instead of the ground radiance spectra generated by ISAC. The linear relationship between the generated and measured at-aperture radiances is used to determine model correction factors. Using simulated data, we demonstrate the capability of this technique to substantially reduce calibration error effects in the corrected atmospheric spectra and retrieved emissivities.**

***Index Terms*—Hyperspectral imaging, remote sensing, calibration.**

I. Introduction

REMOTE sensing in the long-wave infrared (LWIR) portion of the electromagnetic spectrum is important for the retrieval of ground temperature and emissivity. Ground temperature is a key input in climatology models, and material emissivity, which describes a material's ability to emit radiation, is used to identify resources such as minerals. The LWIR region, from 8 to 13 μm, is chosen because it is an atmospheric window with relatively high transmittance. Retrieval of the ground emitted radiance requires removal of atmospheric absorption and emission phenomena, in a process known as atmospheric compensation (AC) [1]. Atmospheric models explain the physical properties of the atmosphere with vertical temperature and gas concentration profiles, which are used with a radiative transfer code, such as MODerate resolution atmospheric TRANsmission (MODTRAN)® to generate transmittance and emission path radiance spectra [2]. The generated atmospheric model transmittance and emission spectra are then used for AC. LWIR hyperspectral imagers are able to measure the radiance at over a hundred narrow contiguous bands forming a spectrum for each spatial pixel. This fine spectral resolution is able to measure the sharp spectral features of the scene's atmosphere, and can be used to determine an atmospheric model for AC. However, the whole AC and emissivity retrieval processes are extremely sensitive to errors in the atmospheric model and the sensor calibration.

The main difficulty of AC lies in the accurate estimation of the scene's atmosphere. Typically, AC algorithms assume that the ground scene area is small enough to ensure that the atmosphere is horizontally homogeneous across the scene. The AC algorithm then determines a single atmospheric model for the entire scene, which is then used to convert the at-aperture radiance spectra of each pixel to ground radiance. The accuracy of the final ground radiance estimates are determined by the accuracy of the atmospheric parameter estimates. There are in-scene and model-based techniques available to find the atmosphere of a scene, of which we propose making a hybrid that reduces the limitations of each.

In-scene AC (ISAC) uses the crucial assumptions that perfect blackbodies can be found within the scene, and there is a perfectly clear band to estimate the ground temperature. With these assumptions, estimates of the ground radiances can be generated for the blackbody pixels, and the linear relationship between the ground and at-aperture radiances can be exploited to find the atmospheric transmittance and upwelling radiance. Since the atmospheric parameters are derived directly from the data, they are automatically at the current sensor calibration. Deviation of the blackbodylike pixels from perfect blackbodies introduces a shape error into the atmospheric estimates [3], meaning an ISAC technique must effectively find the best blackbodylike pixels. The search techniques used in [1] and [4] find blackbodylike

Manuscript received September 24, 2019; revised December 13, 2019; accepted January 3, 2020. Date of publication February 5, 2020; date of current version February 18, 2020. This work was supported by the Air Force Research Laboratory under Air Force Contract #FA8721-05-C-0002. *(Corresponding author: Michael Pieper.)*

M. Pieper, D. Manolakis, and E. Truslow are with MIT Lincoln Laboratory, Lexington, MA 02420 USA (e-mail: mpieper@ll.mit.edu; dmanolakis@ll.mit.edu; Eric.Truslow@ll.mit.edu).

A. Weisner and R. Bostick are with National Air and Space Intelligence Center, Wright-Patterson AFB, OH 45433 USA (e-mail: andrew.weisner@us.af.mil; randall.bostick@us.af.mil).

T. Cooley is with Space Vehicles Directorate, Air Force Research Laboratory, Kirtland AFB, NM 87117 USA (e-mail: thomas.cooley.3@us.af.mil).

Digital Object Identifier 10.1109/JSTARS.2020.2968044

pixels by making band scatter plots for all the pixels that share the most common maximum brightness temperature band, then apply a linear fitting to the top of each scatter plot. The pixels with the minimum variation in their brightness temperatures are used in [5]. Converting a scene to ground radiance using an initial ISAC estimate made with the blackbodylike pixels found with one of the previous techniques, the work in [6] finds blackbodylike pixels that are overcorrected and have absorption features with negative concavity. We determined that using the minimum brightness temperature variance followed by the negative concavity technique was most effective at finding blackbodylike pixels. ISAC has several significant limitations. In order to work effectively, a scene requires an adequate amount of blackbodylike pixels consisting of vegetation or water, which is highly unlikely in arid deserts. In addition, it only provides the atmospheric parameters needed for AC, a model is still required for the downwelling radiance to retrieve the emissivity.

Model-based methods attempt to find an atmospheric model that provides the best atmospheric correction and emissivity estimates. If a model is used to convert the scene to ground radiance, then a technique known as temperature emissivity estimation (TES) is used to determine the emissivity of reflective pixels. The most widely used hyperspectral TES technique makes the assumption that the emissivity spectra of solids are smooth with respect to wavelength, in contrast to the sharp single band absorption features in the atmospheric transmittance. The temperature and emissivity of a pixel are determined by finding the temperature that provides the smoothest emissivity estimate [4]. A model is chosen for a scene based on the smoothness of the emissivity spectra it retrieves for reflective pixels. Algorithms that utilize emissivity spectral smoothness to find the correct model are the automatic retrieval of temperature and emissivity using spectral smoothness (ARTEMISS) [4], [7] and fast line-of-sight atmospheric analysis of spectral hypercubes infrared (FLAASH-IR) [8]. These model-based algorithms are extremely sensitive to calibration errors because they are completely model based and even slight errors can cause the TES smoothness technique to fail. To mitigate calibration errors, these algorithms use calibration correction techniques.

In this article, we describe an in-scene calibration correction technique similar to ISAC, which can be applied to the transmittance and emission spectra generated from the atmospheric model determined for a scene. Combining model-based and in-scene techniques allows us to benefit from the inherent calibration of in-scene methods while not requiring the blackbody assumption due to the atmospheric knowledge from the model.

II. Background

An understanding of the components of the measured at-aperture radiance is required to understand the retrieval process of the ground material emissivity. The monochromatic at-aperture radiance of a simplified radiative transfer model with a single Lambertian surface material is

$$L_{\mathrm{S}}(\lambda) = L_{\mathrm{G}}(\lambda)\tau(\lambda) + L_{\mathrm{U}}(\lambda) \tag{1a}$$

$$L_{\mathrm{G}}(\lambda) = \underbrace{\epsilon_{\mathrm{G}}(\lambda)B(\lambda;T_{\mathrm{G}})}_{\text{Emitted}} + \underbrace{[1-\epsilon_{\mathrm{G}}(\lambda)]L_{\mathrm{D}}(\lambda)}_{\text{Reflected}} \tag{1b}$$

where λ is the wavelength, $L_{\mathrm{G}}(\lambda)$ is the ground radiance, $\epsilon_{\mathrm{G}}(\lambda)$ is the ground emissivity, T_{G} is the ground temperature, $B(\lambda;T_{\mathrm{G}})$ is the emitted energy from a blackbody at T_{G} determined by the Planck function, $L_{\mathrm{D}}(\lambda)$ is the hemispherical downwelling radiance emitted by the atmosphere, $L_{\mathrm{U}}(\lambda)$ is the upwelling path radiance emitted by the atmosphere, and $\tau(\lambda)$ is the atmospheric transmittance. All radiance measurements are in units of μ flicks ($\mu\mathrm{W/cm^2/sr/}\mu\mathrm{m}$). In the majority of cases, the amount of scattered radiance in the LWIR is insignificant, and is therefore ignored. The model assumes a clear sky, however, emitted radiance from clouds above the sensor could be included with the downwelling radiance.

A grating-based hyperspectral sensor with K bands measures a band-averaged version of $L_{\mathrm{S}}(\lambda)$, where band averaging for any radiance component $L(\lambda_k)$ at the kth band is

$$L(\lambda_k) = \langle L(\lambda)\rangle_k = \int S_k(\lambda)L(\lambda)d\lambda \tag{2a}$$

$$S_k(\lambda) = \mathcal{N}(\lambda_k, \sigma_k) \tag{2b}$$

$$\sigma_k = \mathrm{FWHM}_k/(2\sqrt{2\ln 2}) \tag{2c}$$

where $S_k(\lambda)$ is a Gaussian spectral response function (SRF) for band k with a band center wavelength of λ_k, standard deviation σ_k, and band full width half max FWHM_k. The band-averaged at-sensor signal model for the kth band is

$$L_{\mathrm{S}}(\lambda_k) = \epsilon_{\mathrm{G}}(\lambda_k)B_\tau(\lambda_k;T_{\mathrm{G}}) + [1-\epsilon_{\mathrm{G}}(\lambda_k)]L_{\mathrm{D}\tau}(\lambda_k) + L_{\mathrm{U}}(\lambda_k) \tag{3}$$

where the band-averaged parameters are $\epsilon_{\mathrm{G}}(\lambda_k) = \langle\epsilon_{\mathrm{G}}(\lambda)\rangle_k$, $L_{\mathrm{S}}(\lambda_k) = \langle L_{\mathrm{S}}(\lambda)\rangle_k$, $L_{\mathrm{U}}(\lambda_k) = \langle L_{\mathrm{U}}(\lambda)\rangle_k$, $B_\tau(\lambda_k;T_{\mathrm{G}}) = \langle B(\lambda;T_{\mathrm{G}})\tau(\lambda)\rangle_k$, and $L_{\mathrm{D}\tau}(\lambda_k) = \langle L_{\mathrm{D}}(\lambda)\tau(\lambda)\rangle_k$. $L_{\mathrm{D}\tau}(\lambda_k)$ is the ground component of the at-aperture radiance when there is a perfect reflector on the ground [9].

The ground radiance is retrieved from the at-aperture radiance spectrum by removing the effects of atmospheric transmittance loses and emissions in a process known as AC. The at-aperture to ground radiance conversion is

$$L_{\mathrm{G_{AC}}}(\lambda_k) = \frac{L_{\mathrm{S}}(\lambda_k) - L_{\mathrm{U}}(\lambda_k)}{\tau(\lambda_k)} \tag{4a}$$

$$L_{\mathrm{G_{AC}}}(\lambda_k) = \epsilon_{\mathrm{G}}(\lambda_k)B(\lambda_k;T_{\mathrm{G}}) + [1-\epsilon_{\mathrm{G}}(\lambda_k)]L_{\mathrm{D_{AC}}}(\lambda_k) \tag{4b}$$

$$L_{\mathrm{D_{AC}}}(\lambda_k) = L_{\mathrm{D}\tau}(\lambda_k)/\tau(\lambda_k) \tag{4c}$$

where $L_{\mathrm{U}}(\lambda_k)$ and $\tau(\lambda_k)$ have been found with a model-based technique. There is a slight error in $L_{\mathrm{G_{AC}}}(\lambda_k)$ compared to $L_{\mathrm{G}}(\lambda_k)$ from $\tau(\lambda_k)$ not being completely removed from $L_{\mathrm{D}\tau}(\lambda_k)/\tau(\lambda_k)$ due to the band-averaging error.

III. Temperature Emissivity Separation

When the correct atmospheric model is found and band averaged with the current sensor SRF, emissivity retrieval is an underdetermined problem where $\hat{T}_{\mathrm{G}}$ and $\hat{\epsilon}_{\mathrm{G}}(\lambda_k)$ need to be estimated concurrently. Using the assumption that the thermal infrared spectra of solids tend to be smooth, compared to the sharp features of the atmospheric gases, TES algorithms find $\hat{T}_{\mathrm{G}}$ where $\hat{\epsilon}_{\mathrm{G}}(\lambda_k)$ is smoothest [4].

After accurate conversion of the at-aperture radiance to ground radiance using (4a), TES can be done directly on

$L_{\mathrm{G_{AC}}}(\lambda_k)$. Given an estimate of the ground temperature $\hat{T}_{\mathrm{G}}$ the calculated ground emissivity estimate $\hat{\epsilon}_{\mathrm{G}}(\lambda_k)$ is

$$\hat{\epsilon}_{\mathrm{G}}(\lambda_k) = \frac{L_{\mathrm{G_{AC}}}(\lambda_k) - L_{\mathrm{D_{AC}}}(\lambda_k)}{W(\lambda_k, \hat{T}_{\mathrm{G}})} \tag{5a}$$

$$W(\lambda_k, \hat{T}_{\mathrm{G}}) = B(\lambda_k; \hat{T}_{\mathrm{G}}) - L_{\mathrm{D_{AC}}}(\lambda_k) \tag{5b}$$

where $W(\lambda_k, \hat{T}_{\mathrm{G}})$ is the conversion factor from radiance to emissivity [4], [10]. The simplified emissivity estimate is

$$\hat{\epsilon}_{\mathrm{G}}(\lambda_k) = \epsilon_{\mathrm{G}}(\lambda_k)\left(\frac{B(\lambda_k; T_{\mathrm{G}}) - L_{\mathrm{D_{AC}}}(\lambda_k)}{W(\lambda_k, \hat{T}_{\mathrm{G}})}\right) \tag{6}$$

where the smoothness of the emissivity estimate is determined by the fraction in parenthesis. As $\hat{T}_{\mathrm{G}}$ deviates from T_{G}, this fraction deviates from one and becomes rougher, with sharp features from $L_{\mathrm{D_{AC}}}(\lambda_k)$ becoming visible.

Since the true spectrum $\epsilon_{\mathrm{G}}(\lambda_k)$ is not available, we determine the smoothness of $\hat{\epsilon}_{\mathrm{G}}(\lambda_k)$ using a smoothed estimate $\hat{\epsilon}^{\mathrm{s}}_{\mathrm{G}}(\lambda_k)$ in place of $\epsilon_{\mathrm{G}}(\lambda_k)$. The smoothing error is

$$\delta\epsilon_{\mathrm{G}}(\lambda_k) = \hat{\epsilon}_{\mathrm{G}}(\lambda_k) - \hat{\epsilon}^{\mathrm{s}}_{\mathrm{G}}(\lambda_k) \tag{7}$$

where $\hat{\epsilon}^{\mathrm{s}}_{\mathrm{G}}(\lambda_k)$ is a smoothed emissivity estimate using boxcar averaging. The conversion of the emissivity smoothing error to the radiance "smoothing" root-mean-square error (SRMSE) is

$$E_L(T_{\mathrm{G}}) = \sqrt{\frac{1}{k_2 - k_1 + 1}\sum\nolimits_{k=k_1}^{k_2}\left[\delta\epsilon_{\mathrm{G}}(\lambda_k)W(\lambda_k, \hat{T}_{\mathrm{G}})\right]^2} \tag{8}$$

where k_1 and k_2 are the limits of the spectral bands [4].

The goal is to find the value of $\hat{T}_{\mathrm{G}}$, which provides the minimum SRMSE $\min_{T_{\mathrm{G}}} E_L(T_{\mathrm{G}})$ and uses the corresponding smoothest $\hat{\epsilon}_{\mathrm{G}}(\hat{\lambda}_k)$ for detection and identification [4]. $\hat{T}_{\mathrm{G}}$ that provides the minimum SRMSE is found using any numerical optimization technique with a single variable, such as golden section or gradient descent. We used the MATLAB function *"fminsearch,"* which uses unconstrained nonlinear optimizations starting at an initial $\hat{T}_{\mathrm{G}}$. The SRMSE as a function of temperature was studied, and it was determined that there is a single well-defined minimum for ground temperature within realistic bounds. The initial $\hat{T}_{\mathrm{G}}$ is typically determined by the band with the maximum brightness temperature in $L_{\mathrm{G_{AC}}}(\lambda_k)$. The band brightness temperature is the inverse of the Planck function $B^{-1}(\lambda_k; T_{\mathrm{G}})$, and is the temperature at which a blackbody emits radiance $L_{\mathrm{G_{AC}}}(\lambda_k)$ [1].

IV. In-Scene Atmospheric Model Correction

The atmospheric model spectra are band averaged with a sensor SRF obtained from a preflight spectral and radiometric calibration. However, factors such as mechanical vibration and temperature changes can cause the sensor SRF to change over time. The calibration error depending on sensor quality can change in the across-track direction [11]. Changes in the SRF include band shifts $\mathcal{N}(\lambda_k + \Delta, \sigma_k)$ and band broadening $\mathcal{N}(\lambda_k, s\sigma_k)$. The result in a previously measured SRF is only an estimate of the SRF during collection, specified by $\hat{\lambda}_k$. When the atmospheric model spectra are band averaged with $\hat{\lambda}_k$ and used for AC and TES, these wavelength calibration errors cause a mismatch between the atmospheric model spectra and their at-aperture radiance counterparts. These mismatches add errors to the ground radiances and roughness to the final ground emissivity estimates, amounting to over a degree of angular error in the emissivity [10]. Errors of 0.1 band spacing produces an RMSE in the radiance between 4 and 7 μflicks, which is relatively high compared to typical systems with a noise level less than 2 μflicks [4].

The atmospheric model mismatch from calibration errors is corrected using a method similar to ISAC. ISAC uses the linear relationship between at-aperture radiance and ground radiance estimates for blackbodylike pixels to find estimates of the transmittance and upwelling radiance. In-scene atmospheric model, correction uses the linear relationship of the at-aperture radiance with at-aperture radiance estimates for high emissivity pixels to find a calibration correction for an atmospheric model. High-emissivity pixels are found using the ISAC search method that uses the minimum brightness temperature variance followed by negative concavity [5], [6]. These high emissivity pixels are assumed to contain a single high emissivity background surface material $\epsilon_{\mathrm{B}}(\lambda_k)$, such as vegetation or soil. Using the atmospheric model spectra with calibration error, the at-aperture radiances for these high emissivity pixels are

$$L_{\mathrm{S}}(\hat{\lambda}_k) = \epsilon_{\mathrm{B}}(\hat{\lambda}_k)B(\hat{\lambda}_k; \hat{T}_{\mathrm{G}})\tau(\hat{\lambda}_k) + L_{\mathrm{A}}(\hat{\lambda}_k) \tag{9a}$$

$$L_{\mathrm{A}}(\hat{\lambda}_k) = [1 - \epsilon_{\mathrm{B}}(\hat{\lambda}_k)]L_{\mathrm{D}\tau}(\hat{\lambda}_k) + L_{\mathrm{U}}(\hat{\lambda}_k) \tag{9b}$$

where $\tau(\hat{\lambda}_k)$, $L_{\mathrm{U}}(\hat{\lambda}_k)$, and $L_{\mathrm{D}\tau}(\hat{\lambda}_k)$ are band averaged to the estimated SRF, and $L_{\mathrm{A}}(\hat{\lambda}_k)$ is the combined components for the emitted atmospheric radiance of the pixel. The at-aperture radiance estimates require an estimate of $\epsilon_{\mathrm{B}}(\lambda_k)$ and temperature estimates for each high-emissivity pixel. Since the atmospheric model greatly reduces the number of unknowns, we can identify $\epsilon_{\mathrm{B}}(\lambda_k)$ and avoid the limitations of the ISAC blackbody assumption. The ASTER library is searched for an emissivity spectrum that best matches the high-emissivity pixels [12], and the high-emissivity pixel temperatures are estimated for each emissivity spectrum. Using the highest transmittance band $\hat{\lambda}_R$, the temperature estimate for a high-emissivity pixel is

$$\hat{T}_{\mathrm{G}} = B^{-1}\left(\hat{\lambda}_R; \frac{L_{\mathrm{S}}(\lambda_R) - L_{\mathrm{A}}(\hat{\lambda}_R)}{\epsilon_{\mathrm{B}}(\hat{\lambda}_R)\tau(\hat{\lambda}_R)}\right) \tag{10}$$

where $\epsilon_{\mathrm{B}}(\hat{\lambda}_R)$ is the current emissivity at the clear reference channel. Since the temperature of a pixel is constant across bands, the emissivities calculated for all clear bands $\hat{\lambda}_r$ are

$$\hat{\epsilon}_{\mathrm{B}}(\hat{\lambda}_r) = \frac{L_{\mathrm{S}}(\lambda_r) - L_{\mathrm{A}}(\hat{\lambda}_r)}{B(\hat{\lambda}_r; \hat{T}_{\mathrm{G}})\tau(\hat{\lambda}_r)} \tag{11}$$

where the sum of squares error (SSE) between $\hat{\epsilon}_{\mathrm{B}}(\hat{\lambda}_r)$ and $\epsilon_{\mathrm{B}}(\hat{\lambda}_r)$ will be minimized when the correct emissivity is used. The library signature that has the lowest total SSE for all the high emissivity background pixels is then chosen, along with its corresponding pixel temperatures. This technique provides a rough estimate of the quality of an atmospheric model, and is resilient to calibration errors because the clear bands whose $\tau(\hat{\lambda}_k)$ are several bands from sharp atmospheric absorptive feature bands are chosen.

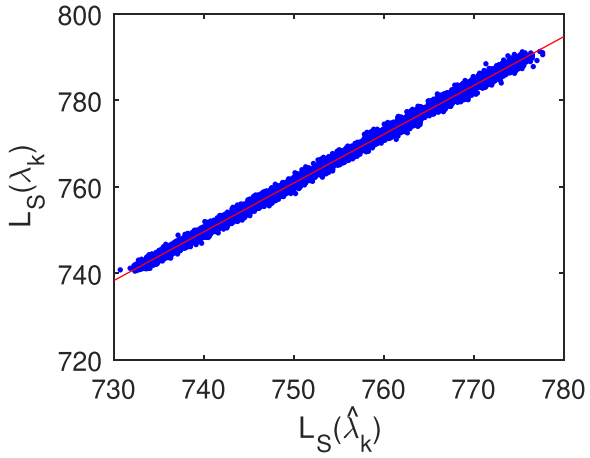

Fig. 1. Band scatter plot and fitting between $L_S(\hat{\lambda}_k)$ and $L_S(\lambda_k)$.

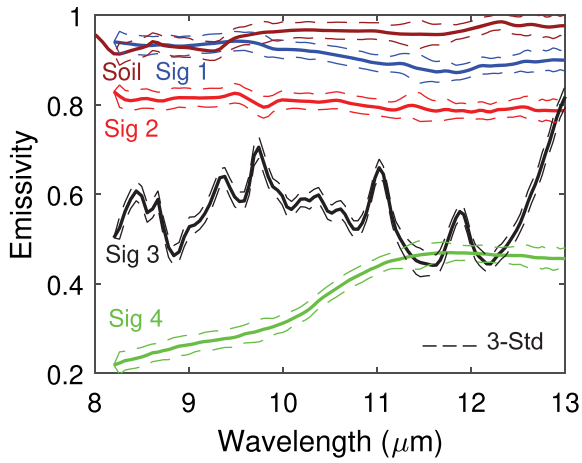

Fig. 2. Emissivity signatures with 3-std variability.

The at-aperture radiance estimates can now be generated for the high-emissivity pixels, and used to create band scatter plots of $L_S(\hat{\lambda}_k)$ (x) versus $L_S(\lambda_k)$ (y), as shown in Fig. 1. Similarly to ISAC, a linear fitting is applied to each band scatter plot to find correction factors between the measured at-aperture radiances and their estimates. With the assumptions that $\epsilon_B(\lambda_k) \approx \epsilon_B(\hat{\lambda}_k)$ and $B(\lambda_k; T_G) \approx B(\hat{\lambda}_k; T_G)$, the calibration error in the atmospheric spectra is the only significant source of error. The resulting calibration correction factors are the transmittance correction $a_\tau(\lambda_k)$ (slope) and emitted atmospheric radiance correction $a_A(\lambda_k)$ (intercept). The final corrected transmittance $\tau^c(\lambda_k)$ and corrected emitted atmospheric radiance $L_A^c(\lambda_k)$ are

$$\tau^c(\lambda_k) = \tau(\hat{\lambda}_k) a_\tau(\lambda_k) \approx \tau(\lambda_k) \tag{12a}$$

$$L_A^c(\lambda_k) = L_A(\hat{\lambda}_k) a_\tau(\lambda_k) + a_A(\lambda_k) \approx L_A(\lambda_k). \tag{12b}$$

The main limitation of this method are correction factors that are only found for $\tau(\hat{\lambda}_k)$ and $L_A(\hat{\lambda}_k)$, which are used for AC to obtain the ground radiance. A separate method is required to correct $L_{D\tau}(\hat{\lambda}_k)$ from reflective ground radiance spectra. In addition, while $\tau(\hat{\lambda}_k)$ can be corrected individually, the calibration errors for the reflected downwelling radiance component cannot be decoupled from those of $L_U(\hat{\lambda}_k)$ in $L_A(\hat{\lambda}_k)$. If $\epsilon_B(\lambda_k)$ is high enough, the calibration error from the downwelling radiance will be negligible, and the corrected $L_U(\hat{\lambda}_k)$ is

$$L_U^c(\lambda_k) = L_U(\hat{\lambda}_k) a_\tau(\lambda_k) + a_A(\lambda_k) \tag{13a}$$

$$\approx L_U(\lambda_k) + [1 - \epsilon_B(\lambda_k)](L_{D\tau}(\lambda_k) - L_{D\tau}(\hat{\lambda}_k) a_\tau(\lambda_k)) \tag{13b}$$

where the second term is the calibration error from the reflected downwelling radiance.

We remove the effects of the reflected downwelling calibration error by keeping the emitted atmospheric radiance components together. The AC with the corrected atmospheric spectra is

$$L_{G_{AC}}^c(\lambda_k) = \frac{L_S(\lambda_k) - L_A^c(\lambda_k)}{\tau^c(\lambda_k)} \tag{14}$$

where the reflected downwelling component in $L_{G_{AC}}^c(\lambda_k)$ is reduced compared to the true ground radiance. The simplified $L_{G_{AC}}^c(\lambda_k)$ is

$$L_{G_{AC}}^c(\lambda_k) \approx \epsilon_B(\lambda_k) L_{GB}(\lambda_k) \tag{15a}$$

$$L_{GB}(\lambda_k) = \frac{\epsilon_G(\lambda_k)}{\epsilon_B(\lambda_k)} B(\lambda_k; T_G) + \left[1 - \frac{\epsilon_G(\lambda_k)}{\epsilon_B(\lambda_k)}\right] L_{D_{AC}}(\lambda_k) \tag{15b}$$

where $L_{GB}(\lambda_k)$ is a ground radiance where the ground emissivity is relative to $\epsilon_B(\lambda_k)$. Standard TES smoothness techniques can be used on $L_{GB}(\lambda_k)$ to find $\epsilon_G(\lambda_k)/\epsilon_B(\lambda_k)$ for a pixel and scaled by $\epsilon_B(\lambda_k)$ to get the true emissivity. A calibration corrected $L_{D_{AC}}^c(\lambda_k)$ for $L_{D\tau}(\hat{\lambda}_k)/\tau^c(\lambda_k)$ can be found using the $L_{GB}(\lambda_k)$ of reflective pixels [13].

V. Results and Analysis

The in-scene atmospheric model correction was tested on simulated data. The high-emissivity soil spectrum in Fig. 2, from the ASTER JHU soil library, was used to generate background spectra. The dashed 3-std variability in the soil emissivity spectra was modeled using a covariance calculated from the emissivities of a large calibration target consisting of several thousand pixels in a spatially enhanced broadband array spectrograph system (SEBASS) collected after AC and TES. SEBASS is a 128-band LWIR hyperspectral sensor [14]. The covariance explained the material variability, and since it was based on actual data contained noise effects. Random emissivity spectra for 5000 ground pixels were generated from a multivariate normal distribution explained by the covariance and added to the soil spectrum band averaged to the SEBASS SRF. The corresponding ground temperatures for the random emissivities were generated from a uniform distribution over a temperature range of 2–20 K centered at 295 K.

At-aperture radiance spectra were generated for the random soil pixel spectra and temperatures using (3) for the high-atmospheric-transmittance SEBASS sensor bands between 8.25 and 13.1 μm corresponding to bands 11–115 [14]. The

high-resolution (HiRes) atmospheric model spectra used in this article were generated with MODTRAN® using the mid-latitude summer atmospheric profiles with temperature, water, and ozone multipliers of 1, and an at-senor altitude of 5 km. Similar performance was observed using temperature multipliers between 0.94 and 1.06, water multipliers between 0.5 and 1.5, and ozone multipliers between 0.85 and 1.15. Tests with radiosondes also showed similar performance. The HiRes atmospheric model spectra were then band averaged with the SEBASS SRF.

The HiRes atmospheric model spectra from the same MODTRAN model were then band averaged using the SRF with a fractional band shift of -0.25 to 0.25 of the minimum band center distance. The in-scene atmospheric model correction was then used to determine the correct soil spectrum from the soil library, and correct the calibration errors in the atmospheric spectra. The corrected atmospheric spectra were then compared to the spectra at the true SRF using the angular error between spectra. The angular error between spectral vectors x and y is

$$\text{Ang}\left(x(\lambda_k), y(\lambda_k)\right) = \cos^{-1}\left(\frac{\boldsymbol{x}\cdot\boldsymbol{y}}{||\boldsymbol{x}||||\boldsymbol{y}||}\right) \tag{16}$$

where the angular error will be used to compare spectra throughout this article.

The quality of emissivity retrieval with corrected atmospheric spectra was studied using at-aperture radiance spectra generated from signatures 1–4 shown in Fig. 2 with 3-std variability bounds. Emissivity variability spectra were added to each emissivity spectrum to create 500 variable emissivity spectra for each signature. These were then used with ground temperatures of 300 and 315 K. At-aperture radiance spectra were then generated with the ground parameters and the true atmospheric spectra. The corrected atmospheric spectra were used for AC using (14), and TES was then done with $L^{c}_{G_{AC}}(\lambda_k)$ using 5-band boxcar smoothing and $L_{D\tau}(\lambda_k)/\tau^{c}(\lambda_k)$. The true downwelling radiance was used to single out the effects of AC errors on the final emissivity retrieval. The calibration error in the downwelling radiance can be corrected after AC using the roughness of the ground radiances in reflective pixels [13]. The angle error between the retrieved and true emissivity spectra were then compared. In the next two sections, atmospheric correction and emissivity retrieval accuracy are studied for variable band-shift errors with a constant background temperature range and variable background temperature range with a constant band-shift error.

A. Band-Shifts Results and Analysis

In this section, we study the ability of in-scene model correction to correct band shifts of -0.25 to 0.25. The background soil spectra had a temperature range of 10 K. The correction factors for a band shift of 0.25 are shown in Fig. 3. The correction factors are significant near the edges of the atmospheric window, and are negatively correlated due to the negative correlation between absorption and emission. The angular errors of the uncorrected and corrected atmospheric model spectra are shown in Fig. 4. It can be seen that the dashed uncorrected errors increase with a band-shift error, and the solid corrected errors are greatly reduced to a level of approximately 0.1°.

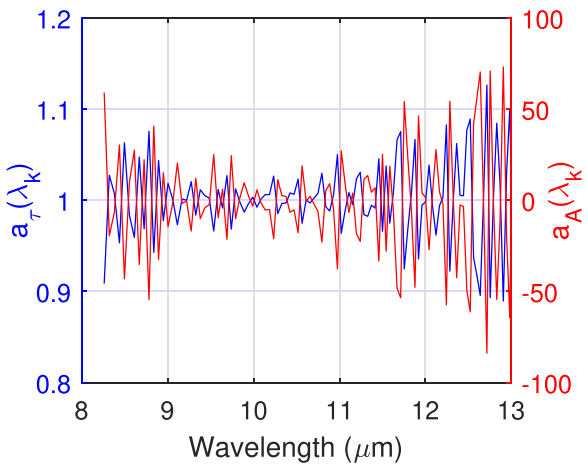

Fig. 3. Atmospheric correction factors over a temperature range of 10 K with a band shift of 0.25.

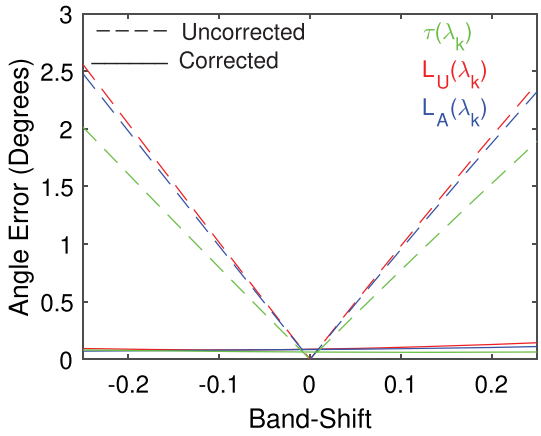

Fig. 4. Angular errors of the corrected and uncorrected atmospheric model spectra over a temperature range of 10 K with varying band shifts.

The quality of the retrieved emissivity spectra for the four signatures using the corrected and uncorrected atmospheric model spectra are shown by the average angular error versus band-shift error in Fig. 5; the rows are for the ground temperatures of 300 and 315 K. The uncorrected atmospheric model spectra had calibration errors in all three spectra. The errors for the dashed uncorrected emissivity spectra increase with the band-shift error and as the signature emissivity decreases. The errors for the corrected spectra show improvement over the uncorrected versus band shift by staying consistent with the uncorrected angular error with no band-shift calibration error.

VI. Temperature Range Results and Analysis

In this section, we study the ability of in-scene model correction to correct a band shift of 0.25, when the background soil spectra range in temperature from 2 to 20 K, with a center temperature 295 K. When the temperature range decreases, the band scatter plots become more spherical and the effects of emissivity variability increase. Deviations in the emissivity from the library spectrum will cause temperature errors and shifts in the x coordinates of pixels in the band scatter plots. Fig. 6

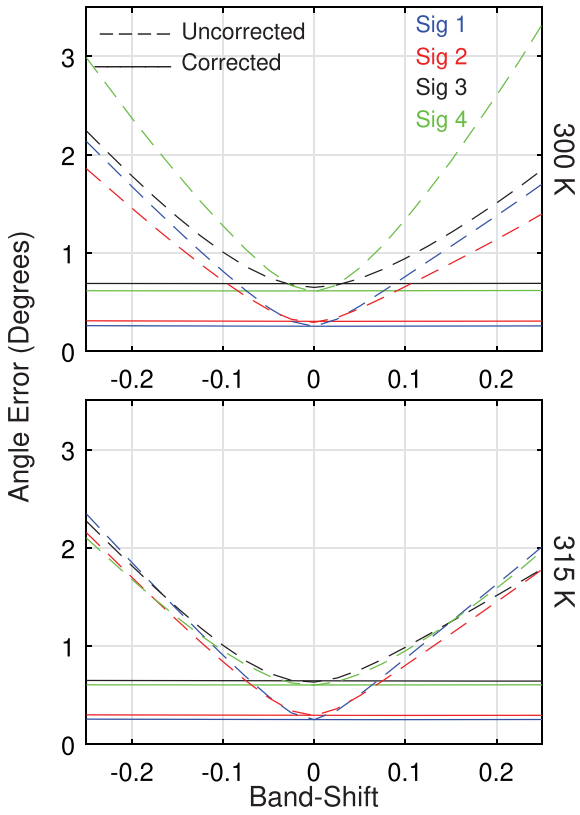

Fig. 5. Angular emissivity errors using the corrected and uncorrected atmospheric model spectra over a temperature range of 10 K with varying band shifts for ground temperatures of 300 and 315 K.

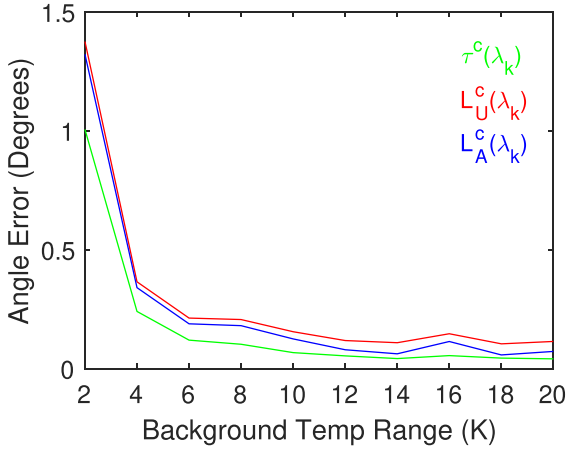

Fig. 6. Angular errors of the corrected atmospheric model spectra over varying background temperature ranges and a band shift of 0.25.

shows the angle error for the corrected spectra versus the background temperature range. The errors remain relatively constant down to a temperature range of 5 K, and then quickly increase. At this temperature range, the effects of the emissivity variability in the band scatter plots are significant compared to the temperature range.

The average angular errors of the retrieved emissivity spectra for the four signatures and two ground temperatures using the corrected atmospheric model spectra found over varying background temperature ranges are shown in Fig. 7. As expected,

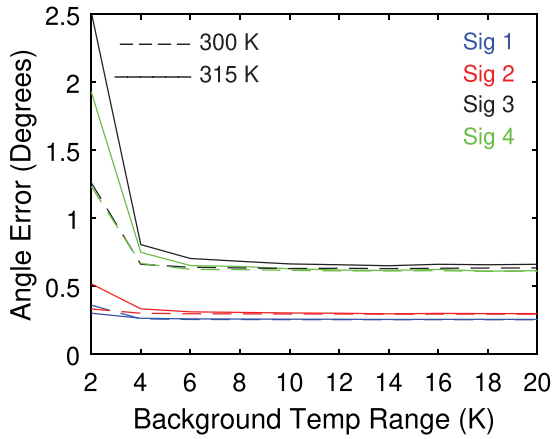

Fig. 7. Angular emissivity errors over varying background temperature ranges and a band shift of 0.25.

the angular errors are nearly constant down to a range of 5 K matching the corrected errors in Fig. 6, and they quickly increase below that. The amount of error for the high-emissivity signatures remains relatively insignificant.

VII. Conclusion

In-scene atmospheric model correction was shown to consistently correct the atmospheric model spectra to within roughly 0.1° of the truth with a band-shift error. Assuming a downwelling radiance without a calibration error, emissivities retrieved with the corrected atmospheric model spectra are nearly identical to when no calibration error is present. It was shown that a correction robust to emissivity variability and temperature estimation requires the linear fitting over a background temperature range of at least 5 K. Below 5 K, the corrected atmospheric model spectra and retrieved emissivities quickly show large errors.

Acknowledgment

Opinions, interpretations, conclusions, and recommendations are those of the authors and are not necessarily endorsed by the United States Government.

References

[1] S. J. Young, B. R. Johnson, and J. A. Hackwell, "An in-scene method for atmospheric compensation of thermal hyperspectral data," *J. Geophys. Res., Atmos.*, vol. 107, no. D24, pp. ACH 14-1–ACH 14-20, 2002.

[2] A. Berk, P. Conforti, R. Kennett, T. Perkins, F. Hawes, and J. van den Bosch, "MODTRAN6: A major upgrade of the MODTRAN radiative transfer code," in *Algorithms and Technologies for Multispectral, Hyperspectral, and Ultraspectral Imagery XX*, vol. 9088, M. Velez-Reyes and F. A. Kruse, Eds. Bellingham, WA, USA: SPIE, 2014, pp. 113–119.

[3] M. Pieper, "Atmospheric compensation and surface temperature and emissivity retrieval with LWIR hyperspectral imagery," Ph.D. dissertation, Dept. Elect. Comput. Eng., Northeastern Univ., Boston, MA, USA, 2017.

[4] C. Borel, "Error analysis for a temperature and emissivity retrieval algorithm for hyperspectral imaging data," *Int. J. Remote Sens.*, vol. 29, no. 17/18, pp. 5029–5045, 2008.

[5] L. Bernstein, J. Gelbord, S. Adler-Golden, N. Guler, R. Sundberg, and P. Conforti, "An improved in-scene atmospheric retrieval and correction algorithm for long-wavelength infrared hyperspectral imagery," *Proc. SPIE*, vol. 10768, 2018, Art. no. 107680J.

[6] M. Boonmee, "Land surface temperature and emissivity retrieval from thermal infrared hyperspectral imagery," Ph.D. dissertation, Chester F. Carlson Center for Imaging Science (COS), Rochester Inst. Technol., Rochester, NY, USA, 2007.
[7] C. C. Borel and R. F. Tuttle, "Recent advances in temperature-emissivity separation algorithms," in *Proc. Aerosp. Conf.*, Mar. 2011, pp. 1–14.
[8] S. M. Adler-Golden, P. Conforti, M. Gagnon, P. Tremblay, and M. Chamberland, "Long-wave infrared surface reflectance spectra retrieved from Telops Hyper-Cam imagery," *Proc. SPIE*, vol. 9088, 2014, Art. no. 90880U.
[9] P. M. Ingram and A. H. Muse, "Sensitivity of iterative spectrally smooth temperature/emissivity separation to algorithmic assumptions and measurement noise," *IEEE Trans. Geosci. Remote Sens.*, vol. 39, no. 10, pp. 2158–2167, Oct. 2001.
[10] M. Pieper *et al.*, "Effects of wavelength calibration mismatch on temperature-emissivity separation techniques," *IEEE J. Sel. Topics Appl. Earth Observ. Remote Sens.*, vol. 11, no. 4, pp. 1315–1324, Apr. 2018.
[11] L. Guanter, R. Richter, and J. Moreno, "Spectral calibration of hyperspectral imagery using atmospheric absorption features," *Appl. Opt.*, vol. 45, pp. 2360–2370, Apr. 2006.
[12] A. M. Baldridge, S. J. Hook, C. I. Grove, and G. Rivera, "The ASTER spectral library: Version 2.0," *Remote Sens. Environ.*, vol. 113, pp. 711–715, 2009.
[13] M. Pieper *et al.*, "Wavelength calibration correction for ground radiance spectra in LWIR hyperspectral imagery," in *Proc. SPIE*, 2018, Art. no. 1076805.
[14] D. W. Warren, J. A. Hackwell, and D. J. Gutierrez, "Compact prism spectrographs based on aplanatic principles," *Opt. Eng.*, vol. 36, no. 4, pp. 1174–1182, 1997.

Michael Pieper received the B.S. and M.S. degrees in 2007 and the Ph.D. degree in 2017 from Northeastern University, Boston, MA, USA, all in electrical engineering.

He is currently a Technical Staff Member with MIT Lincoln Laboratory, Lexington, MA, USA. His research interests include atmospheric compensation, detection, identification, and temperature–emissivity separation in hyperspectral imaging remote sensing.

Dimitris Manolakis (Life Fellow, IEEE) received the B.S. degree in physics and Ph.D. degree in electrical engineering from the University of Athens, Athens, Greece, in 1976 and 1981, respectively.

He is currently a Senior Staff Member with the Massachusetts Institute of Technology (MIT) Lincoln Laboratory, Lexington, MA, USA. He is a co-author of the textbooks *Digital Signal Processing: Principles, Algorithms, and Applications*, 4th Ed. (Prentice-Hall, 2006), *Statistical and Adaptive Signal Processing* (Artech House, 2005), *Applied Digital Signal Processing* (Cambridge University Press, 2011), and *Hyperspectral Imaging Remote Sensing* (Cambridge University Press, 2016).

Eric Truslow received the B.S. degree in electrical engineering from Union College, Schenectady, NY, USA, and the M.S. and Ph.D. degrees from Northeastern University, Boston, MA, USA, in 2010, 2012 and 2015, respectively.

He is currently a Technical Staff Member with MIT Lincoln Laboratory, Lexington, MA, USA. His research interests include chemical vapor detection in hyperspectral data and statistical modeling of hyperspectral imagery.

Andrew Weisner received the B.S. and M.S. degrees in chemistry from Wright State University, Dayton, OH, USA, in 2001 and 2003, respectively.

He is currently a Chemist, working in the field of spectral data exploitation with the U.S. Air Force National Air and Space Intelligence Center, Wright-Patterson AFB, OH, USA.

Randall Bostick received the B.S. degree in mathematics and the M.S. degree in physics from Wright State University, Dayton, OH, USA, and the Ph.D. degree in electro-optical sciences from the Air Force Institute of Technology, Wright-Patterson AFB, OH, USA, in 1990, 1997 and 2013, respectively.

He is currently an Image Scientist, working in the field of spectral data exploitation with the U.S. Air Force National Air and Space Intelligence Center, Wright-Patterson AFB.

Thomas Cooley received the B.S. degree in electrical engineering from Rensselaer Polytechnic Institute, Troy, NY, USA, in 1988, the M.S. degree in electrical engineering and applied physics from the California Institute of Technology, Pasadena, CA, USA, in 1991, and the Ph.D. degree in optical sciences from The University of Arizona, Tucson, AZ, USA, in 1995.

He is currently a Member of the scientific and technical cadre of senior executives and the Chief Scientist with the Space Vehicles Directorate, Air Force Research Laboratory, Air Force Materiel Command, Kirtland AFB, NM, USA. He was the Principal Investigator of the Artemis payload, a hyperspectral sensor to demonstrate the use of this rich data source for the wide range of applications, and a Program Manager for the TacSat-3 satellite launched in May 2009. He is a co-author of the textbook *Hyperspectral Imaging Remote Sensing* (Cambridge University Press, 2016).